Heliyon 9 (2023) e20548

Contents lists available at ScienceDirect

Heliyon

journal homepage: www.cell.com/heliyon

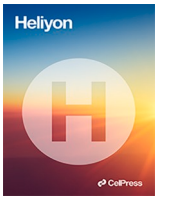

Synthesis of silver nanoparticles for use in conductive inks by chemical reduction method

Ehsan Naderi-Samani *, Reza Shoja Razavi, Khanali Nekouee, Hamed Naderi-Samani

Faculty of Materials and Manufacturing Technologies, Malek Ashtar University of Technology, Iran

ARTICLE INFO

Keywords:
Silver nanoparticles
Chemical reduction
Silver conductive ink
Printed electronics
PVP
Hydrazine

ABSTRACT

In this study, the chemical reduction method was applied to synthesize silver nanoparticles used to prepare conductive inks. The two variables of polyvinylpyrrolidone (PVP)-*stabilized* mole in the 0.01–0.03 mol range and hydrazine reducing mole in the 0.1–0.5 mol range, along with constants such as precursor mole (silver nitrate), complexing mole (ethylene diamine) and solvent mole (water), were used. Nine random samples proposed by the Design Expert software were examined and studied. X-ray diffraction (XRD) patterns, field emission scanning electron microscopy (FE-SEM), transmission electron microscopy (TEM) and dynamic light scattering (DLS) were then used to characterize and evaluate the synthesized nanoparticles. According to the results obtained by XRD, FE-SEM and TEM analyses, the sample with 0.025 mol and 0.3 mol PVP had the minimum size of silver nanoparticles, which was around 20 nm, so it was chosen as the optimal sample for further research. The conductive ink was also prepared with the optimal sample of silver nanoparticles in 40% by weight and then characterized and evaluated by applying ultraviolet–visible (UV–Vis), simultaneous thermal analysis (STA), FE-SEM and electrical conductivity analysis. Finally, conductive ink was applied to polyethylene terephthalate (PET) and acrylonitrile butadiene styrene (ABS) substrates. The surface electrical resistance of conductive ink on PET and ABS substrates was then measured at about 6.4 Ω and 2.2 Ω, respectively.

1. Introduction

Since the advent of electronic printing technology, obtaining electrically conductive ink has been one of the most important targets [1]. Electronic printing technology is developing at a noteowrthy speed; today it has received the attention of the world industry and trade. One of the main reasons for the development of electronic printing technology is the rise of the global demand for flexible and lightweight electronic components. The production of electronic components using electronic printing technology increases the production speed and efficiency, reduces environmental pollution, and decreases the production costs. One of the most important advantages of electronic printing technology is its ability to produce electronic parts on multiple substrates, such as fabric, paper, plastic, metal, etc., leading to its widespread use in many fields [2]. Electronic printing technology has evolved in the course of time; today, the production of electronic components is widely carried out using silk screen printing and inkjet printing methods [3].

In the silk screen printing method, the desired pattern is printed by placing the substrate under the stencil and spreading the conductive ink on it; it is one of the contact printing methods. In the inkjet printing method, the ink in the printer's ink tank enters a part called the head through special hoses; then the head puts the ink on the paper based on the points in the printing order. Inkjet

* Corresponding author.
E-mail address: ehsan.n.samani75@mut.ac.ir (E. Naderi-Samani).

https://doi.org/10.1016/j.heliyon.2023.e20548
Received 10 May 2023; Received in revised form 27 August 2023; Accepted 28 September 2023
Available online 29 September 2023

printing is considered one of the non-contact printing methods [4].

Due to the widespread use of electronic printing technology in many fields, such as transportation, medicine, aerospace, smart clothing and defense industries, according to global statistics, its revenue has risen from 3.05 in 2015 to 10.26 billion dollars in 2021. Therefore, electronic printing technology has become a growing and developing technology [5]. One of the most important characteristics of conductive inks is their electrical conductivity. Their other characteristics are stability, good adhesion to the substrate and suitable mechanical properties (flexibility). At first, the conductive ink containing conductive polymers, silicon or other semiconductors was used. Due to the limited electrical conductivity of inks containing semi-conducting materials and conducting polymers, those including carbon materials were replaced. However, some factors limiting the use of carbon inks are their low stability, their tendency to clump and their limited electrical conductivity [6].

With the growing demand in the industry and the need for high electrical conductivity, inks containing metals have received attention and considerable research has been done to develop them. In global trade, due to the rise of demand, a significant increase of the revenue from the business of conductive inks is predicted [7]. Due to its economic efficiency, no need for expensive equipment and favorable efficiency, the chemical reduction method has been used. From the synthesis of components by the chemical reduction method of the precursor (silver nitrate and silver oxalate, etc.), solvent (water, ethanol, ethylene glycol, etc.), reducing materials (hydrazine, sodium borohydride ($NaBH_4$), ascorbic acid and sodium hypophosphite, etc.) and stabilizer (PVP and cetyl trimethyl bromide (CTAB) etc.) were employed [[8–10]]. One of the important and significant points regarding synthesis by the chemical reduction method is finding the optimal concentration of each synthesis component and controlling the temperature, mixing speed, etc. [10].

Conductive inks containing metal particles are subjected to sintering after being applied to the substrate, and electrical conductivity is achieved by joining the metal particles and forming a continuous metal layer (the specific electrical resistance of the gold metal layer, the copper layer, and the silver is equal to $2.4 \times 10^{-8}\ \Omega$, $1.7 \times 10^{-8}\ \Omega$, and $1.6 \times 10^{-8}\ \Omega$, respectively). Silver nanoparticles have been considered in applying conductive ink due to their high electrical conductivity and good oxidation resistance. Silver nanoparticles have a oxidation resistance higher than that of copper nanoparticles and a price lower than that of gold nanoparticles. For this reason, silver conductive ink has received much attention. It should be noted that the preparation of the conductive ink with metal particles on a nanoscale leads to good stability and lowers the sintering temperature of the ink [11].

In synthesizing silver nanoparticles, it is important to find the agent or agents that can reduce the size of the nanoparticles to prevent the printer head from closing. In general, it is a serious challenge to make ink with stability combined in the absence of particle aggregation; this, in addition to providing electrical conductivity and suitable mechanical properties, can be used in inkjet printers and does not cause damage to the printer head. Therefore, researchers have conducted many studies in these fields (Table 1) and there are also commercial products (Table 2). The innovation of this study is in the design of nanoparticle synthesis tests with software by stabilizing and reducing the variables and constants of precursor, solvent and complexing agent. The purpose of this study was, therefore, to find the optimal parameters for the synthesis of silver nanoparticles by the chemical reduction method and investigate its use in the production of the conductive ink applied in printed electronics.

2. Materials and methods

2.1. Chemicals as well as materials

The reaction system contained silver nitrate as a silver precursor, ethylenediamine as a complexing agent, polyvinylpyrrolidone (PVP, average molecular weight of 25000) as a stabilizing agent, hydrazine hydrate (H) as a reductant and deionized water as a solvent. All chemicals were purchased from Merck Chemical Co. (Germany) and used without further filtration. Deionized water was provided by Sablan Co. (Tehran, Iran).

Table 1
A summary of the previous studies.

Metal salt	Reducing agent	Capping agent	Solvent	Particle size (nm)	Reference
Silver nitrate	Ethanol	Triethylenetetramine	Ethanol	20	[12]
Silver nitrate	Ethylene Glycol	PVA	Ethanol	10–70	[13,14]
Silver nitrate	Ascorbic Acid	Sodium Citrate	Water	51	[15]
Silver nitrate	Ascorbic Acid	PVA	Water	55–68	[16]
Silver nitrate	Dimethyl Formamide	PVA	Water	25	[17]
Silver nitrate	Sodium Borohydrate	PVP	Water	1–100	[16,18,19]
Silver nitrate	Sodium Borohydrate	Sodium Citrate	Water	38	[20]
Silver nitrate	Sodium Borohydrate	Chitosan	Water	10	[21]
Silver nitrate	Triethanolamine	PVP	Water	40–43	[22]
Silver nitrate	Formaldehyde	PVA	Water	5–20	[23]
Silver acetate	Phenylhydrazine	Tetraethylpentaamine	Isopropanol	1–2	[24]
Silver chloride	Hydrazine hydrate	PVA	Water	10–60	[25]

Table 2
Commercial silver conductive inks.

Ink	Company	Substrate structure	Curing (°C)	Volume Resistivity (Ω.cm)	Adhesion	Applications	Reference
InkTec-IJ-010	InkTec	Plastics	135	4.2×10^{-6}	5 - 4B	Memory Cell, Display, RFID	[26]
PFI-722	NovaCentrix	PET, Polyimide, Paper	80	5×10^{-6} to 7×10^{-6}	N/A	Sensor, Pharmaceutical Packaging, Solar Cell and Antenna	[27]
DM-SIJ-3200	Dycotec Materials	PET, Polyimide, Paper	100	10×10^{-6}	5B	Sensors, Heaters and solar cell	[28]
PRO-SHIELD 7108	Parker	Plastics	RT	10	N/A	EMI Shielding	[29]

2.2. Test design for the synthesis of silver nanoparticles

Design Expert software (version 11) was used to design the test. To synthesize silver nanoparticles, the volume of the solvent (distilled water) was considered according to the amount of the precursor (silver nitrate). To ensure the complete dissolution of silver nitrate, completion of reactions and easier separation of nanoparticles, a higher amount of the solvent was considered. The amount of the complex agent (ethylenediamine) was also obtained by complexometric titration. In this case, ethylenediamine was added in a dropwise manner to the solution until the reaction was complete and the solution color changed. Therefore, the amounts of precursor (silver nitrate), complexing agent (ethylenediamine) and solvent (deionized water) were fixed and two reducing and stabilizing agents (hydrazine and PVP) were used as the variable agents of the test at five levels. The changes for each of these agents, the upper and lower limit and other relevant information are given in Table 3.

The software randomly presented nine compounds for synthesis. Coding of the samples could be done using variable agents in the composition. The coding of nine samples is given in Table 4. In the coding process, P and H refer to the PVP stabilizer and hydrazine reductant, respectively. For example, in the first sample (P0.01H0.1), 0.01 mol of PVP stabilizer and 0.1 mol of hydrazine were used.

2.3. Synthesis of 9 random samples

At this phase, nine compounds proposed by the Design Expert software were synthesized based on the values presented in Table 4 at room temperature. For the synthesis of each sample, first, 5 g of silver nitrate was completely dissolved in 50 ml of deionized water by a magnetic stirrer for 20 min and at a speed of 500 rpm. Then 5 cc of ethylenediamine was added in a dropwise manner to the mixture and the sample was mixed for 20 min by a magnetic stirrer at 500 rpm. Next, the polymer stabilizer was added to each sample and the solution was subjected to magnetic stirring (500 rpm) for 20 min. In the final phase of synthesis, the hydrazine reductant was also added to the solution and subjected to magnetic stirring (500 rpm) for 15 min. It should be noted that in all these nine samples, the amounts of silver nitrate and ethylene diamine were considered equal to 5 g and 5 cc, respectively. Also, the PVP and hydrazine values (reaction variables) changed in the range of 0.01–0.03 mol and 0.1–0.5 mol, respectively.

After the completion of the synthesis process, the nanoparticles were separated by centrifugation at 8000 rpm. To remove impurities and substances that did not participate in the reaction, the nanoparticles were washed with water and dried at 40 °C (Fig. 1).

2.4. Preparation of the conductive ink from the synthesized silver nanoparticles

After selecting the optimal and appropriate nanoparticles, to prepare the conductive ink containing 40% by weight of silver nanoparticles, they were distributed in the composition of ethylene glycol and ethanol solvents with the volume ratios of 1:2. The prepared ink was subjected to magnetic stirring for 6 h to ensure the optimal stability of silver nanoparticles in the composition of the solvents (Fig. 2).

It should be noted that the prepared conductive ink was stable for two months and had no deposits during this period. In the final phase, the conductive ink was applied on the substrates of PET and ABS by the silk screen printing method with the 150 mesh net and spray method. Thermal sintering of the applied layer was done at 110 °C.

2.5. Characterization and evaluation equipment

To study the morphology of the synthesized nanoparticles, FE-SEM and TEM images were used. XRD was applied to check the

Table 3
Test design information in the Design Expert software.

Variables	Minimum amount (mol)	Maximum amount (mol)
Polyvinylpyrrolidone (PVP)	0.01	0.03
Hydrazine hydrate (H)	0.1	0.5

Table 4
Coding of the samples.

Number of samples	Codings
1	P0.01H0.1
2	P0.03H0.1
3	P0.01H0.5
4	P0.03H0.5
5	P0.015H0.3
6	P0.025H0.3
7	P0.02H0.2
8	P0.02H0.4
9	P0.02H0.3

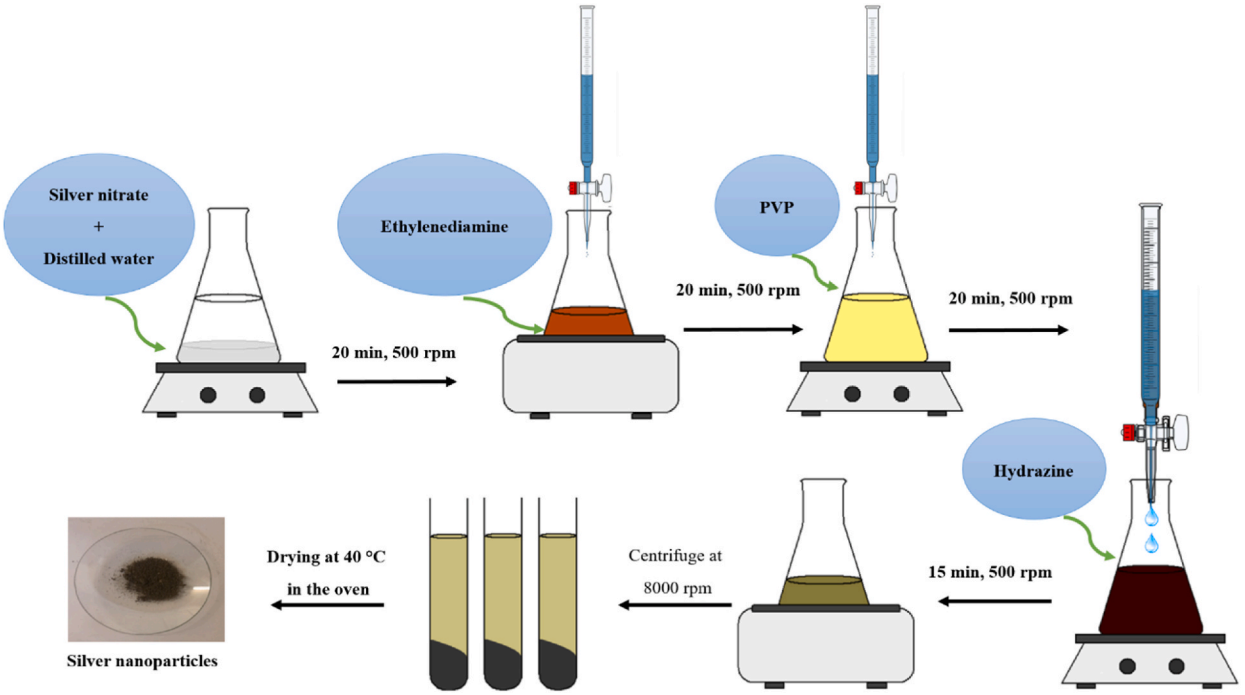

Fig. 1. Schematic of the synthesis phases of silver nanoparticles.

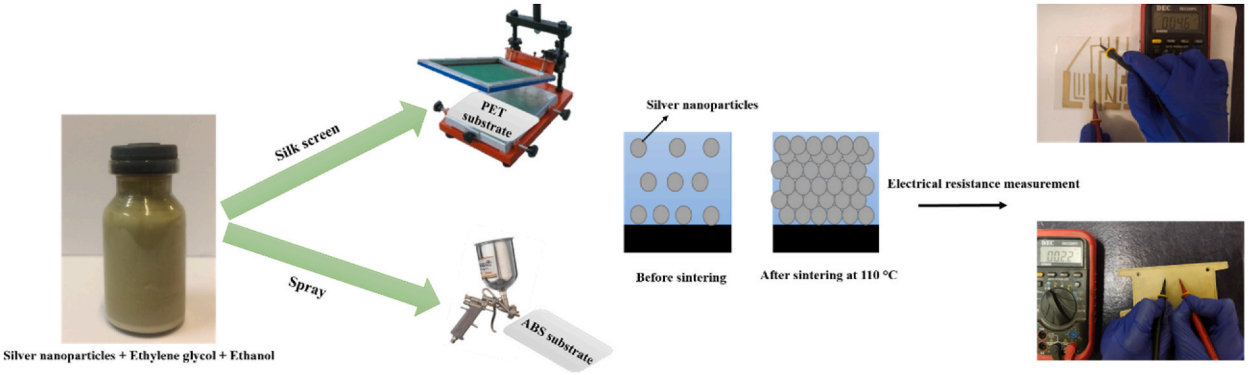

Fig. 2. Schematic of the preparation and printing phases of the conductive ink.

phases and confirm the presence of silver nanoparticles. To confirm the size of nanoparticles and hydrodynamic measurement of nanoparticles, DLS was used.

For the synthesized silver ink, to confirm the presence of silver nanoparticles, UV–Vis was used; to determine the percentage of silver present and the sintering temperature of the ink, STA was applied, which was a composition of differential scanning calorimetry (DSC) and Thermogravimetry Analyzer (TGA). Also, atomic absorption spectroscopy (AAS) was used to determine the concentration of silver in conductive ink accurately. The morphology of the coating and electrical conductivity of the layer were also examined using FE-SEM and digital multimeter, respectively. The samples' adhesion strength test was conducted based on the ASTM D3359 standard by applying the Cross-Cut method; they were utilized to accurately measure the adhesive strength between the ink printed on PET and ABS. To warrant the results of the cross-cut adhesion testing, this test was repeated three times for each sample. Table 5 shows the equipment, purpose of the test, preparation of samples, and the manufacturer and model of the equipment.

3. Results and discussion

3.1. Synthesis of silver nanoparticles

3.1.1. Phase and crystal analysis: XRD pattern

The XRD patterns of the synthesized samples are shown in Fig. 3 (a). According to the sources available in the Expert software, by examining the identification card related to the silver metal phase with the card number (01-087-0719), it was found that the peaks created at the angles of 38.2, 44.4, 64.7, 77.7 and 81.9° were related to the silver metal with the FCC structure and could be located in (111), (200), (220), (311) and (222) crystal planes, respectively. By matching the XRD patterns of the synthesized samples and the standard identification card, it was determined that the synthesized silver nanoparticles were pure and free of any impurities. The absence of the oxide phase in the synthesized samples indicated the good stability of the synthesized silver nanoparticles, despite their nanoscale. On the other hand, the non-formation of the silver oxide phase showed the good performance of the PVP stabilizer and its suitable protection [30].

In addition to the stabilizing effect, ethylene diamine, as a complexing agent, also served an influential role in the absence of the silver oxide phase, since the complexation process was completed and the silver ion complex was formed with the ethylenediamine agent according to the reactions 1 and 2. By adding the hydrazine reductant, reduction to silver metal also took place and no reaction between silver ion and oxygen ion occurred (reaction 3). As a result, the formation of the silver oxide phase could be prevented [[31–34]].

$$Ag^{+} + 6(OH_2) = \left(Ag(OH_2)_6\right)^{+} \tag{1}$$

$$Ag((OH_2))_6 + C_2H_8N_2 = \left(Ag(en)_2\right)^{+}\right) + 4(OH_2) \tag{2}$$

$$\left(Ag(en)_2\right)^{+}\right) + N2H4 = Ag + NO + H^{+} \tag{3}$$

The crystallite size of silver nanoparticles was obtained from the Debye–Scherrer equation, according to equation (4) [35]. In this equation, K = 0.9, λ, β and θ are the shape factor, the X-ray wavelength (equivalent to 1.5406 Å), the full width at half maximum of the

Table 5
Characterization techniques for silver nanoparticles and conductive silver ink.

Techniques	Properties	Preparation of samples	Equipment specifications
FE-SEM	Size and morphology analysis	Distribution of silver nanoparticles in water	Manufacturer: Tescan Device model: MIRA III
TEM	Size and morphology analysis	Distribution of silver nanoparticles in water	Manufacturer: Philips Model: CM120
XRD	Crystal Structure and crystallite size	Drying of nanoparticles at 40 °C in a vacuum oven	Manufacturer: Philips Model: PW173
DLS	Hydrodynamic size analysis and dispersity	Distribution of silver nanoparticles in water	Manufacturer: Horiba Model: SZ-100Z2
UV–Vis	Nanoparticles formation	Conductive ink containing silver nanoparticles	Manufacturer: Analytik Jena Model: SPECORD 210 PLUS
STA	Thermal analysis	Conductive silver ink with a temperature rate of 10°/min in an argon atmosphere	Manufacturer: PerkinElmer Model: STA 6000
AAS	Concentration of nanoparticles	Conductive ink containing silver nanoparticles	Manufacturer: Agilent Model: 240 AA
Multimeter	Electrical resistance	Silver conductive ink printing on PET and ABS substrates	Manufacturer: DEC Model: DEC330FC
Cross-Cut	Adhesion strength	Silver conductive ink printing on PET and ABS substrates	Manufacturer: Elcometer Model: Elcometer 107

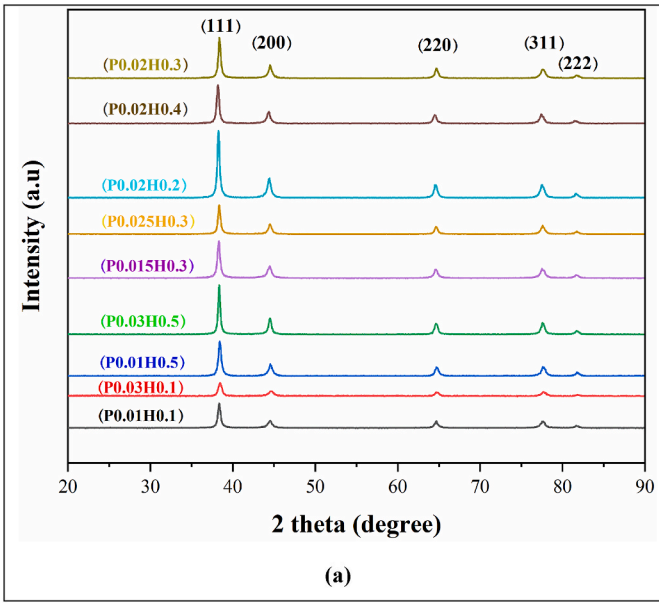

Samples	FWHM (°2θ)	Crystallite size (nm)
P0.01H0.1	0.25	37.4
P0.03H0.1	0.34	27.5
P0.01H0.5	0.29	32.2
P0.03H0.5	0.36	26
P0.015H0.3	0.35	26.7
P0.025H0.3	0.5	18.7
P0.02H0.2	0.3	31.1
P0.02H0.4	0.296	31.5
P0.02H0.3	0.31	30.1

(b)

Fig. 3. a) XRD pattern of the synthesized nanoparticles and b) size of the crystallites obtained from the Debye–Scherrer equation.

diffraction peak, and the angle corresponding to the diffraction peak, respectively. The size of nanoparticle crystallites in different synthesis modes is shown in Fig. 3 (b). The minimum size of the obtained crystallites corresponded to the P0.025H0.3 sample, indicating the suitability of the amount of the reductant and stabilizer, as compared to other samples. Also, the results related the size of the crystallites confirmed the nanocrystalline structure of the nanoparticles.

$$D = \frac{K\lambda}{\beta \operatorname{Cos} \theta} \tag{4}$$

3.1.2. Morphological analysis: FE-SEM images

The morphology and size of nanoparticles were analyzed using FE-SEM images. The images of the synthesized samples are shown in Fig. 4. To identify the optimal sample (with the smallest particle size and narrow grain size distribution), the particle size was recorded using the Digimizer software. Also, the mean and standard deviation of each was calculated. The results of the analyses are also represented in Table 6. From the data analysis and results, it became clear that the size of the synthesized nanoparticles decreased with the increase of the added mole of reductant.

The decrease in the size of the synthesized nanoparticles resulted from the increase in the mole of the reductant, which was, in turn, due to the rise of the initial nucleation of the silver nanoparticles. With the increase of the reductant added at the beginning of the reduction reaction and convertion of silver ions into silver metal, the primary nucleations were formed with a greater amount and intensity. As a result, the size of the synthesized nanoparticles was decreased. Of course, this increase in the mole of the reductant had an optimal value; by increasing the reductant from the optimal state, due to the high nucleation rate, nanoparticles aggregation could occur. In other words, by increasing the mole of the reductant, the power of the reducing agent in the synthesis chamber could be increased, and the silver ions in the reaction medium would be separately and independently converted into silver metal [[36–38]]. This means that the presence of higher amounts of the reducing agent with higher reducing power could lead to the creation of more neutral metal atoms (due to the higher reaction rate) over time and higher nucleation. Higher nucleation due to the limited concentration causes more limited growth of each nucleus and hence, smaller size of nanoparticles [39]. PVP stabilizer has been used to agglomerate silver nanoparticles, causing the collision of them with each other and increasing the size of nanoparticles.

For example, for the sample, with the increase of the added mole of the reductant from 0.1 mol to 0.5 mol (considering the constant mole of the stabilizer at 0.01 mol), the mean size of the synthesized particles was decreased from about 76.11 to 66.94 nm.

The results obtained in this section were compatible with those reported in the literature. Park et al. also observed that the size of the synthesized nanoparticles was decreased with the increase in the concentration of the added reductant, due to the increase in initial nucleation; so, by increasing the mole of the reductant from 12.75 to 19.13 mmol, the size of the synthesized nanoparticles was decreased from 72 to 54 nm [40].

On the other hand, with the increase of the added polymer stabilizer mole in the constant mole of the reductant, the standard deviation of the synthesized samples was also decreased, as increasing the mole of polymer stabilizer led to uniformity in the morphology and size of the synthesized nanoparticles [[20,22,41]]. Regarding various stabilities created in nanoparticles as a result of adding stabilizers, with the rise of the mole of polymer stabilizers, the density of polymer branches around the synthesized nanoparticles increased; as a result, nanoparticles were prevented from colliding with each other and joining together; also, the size of

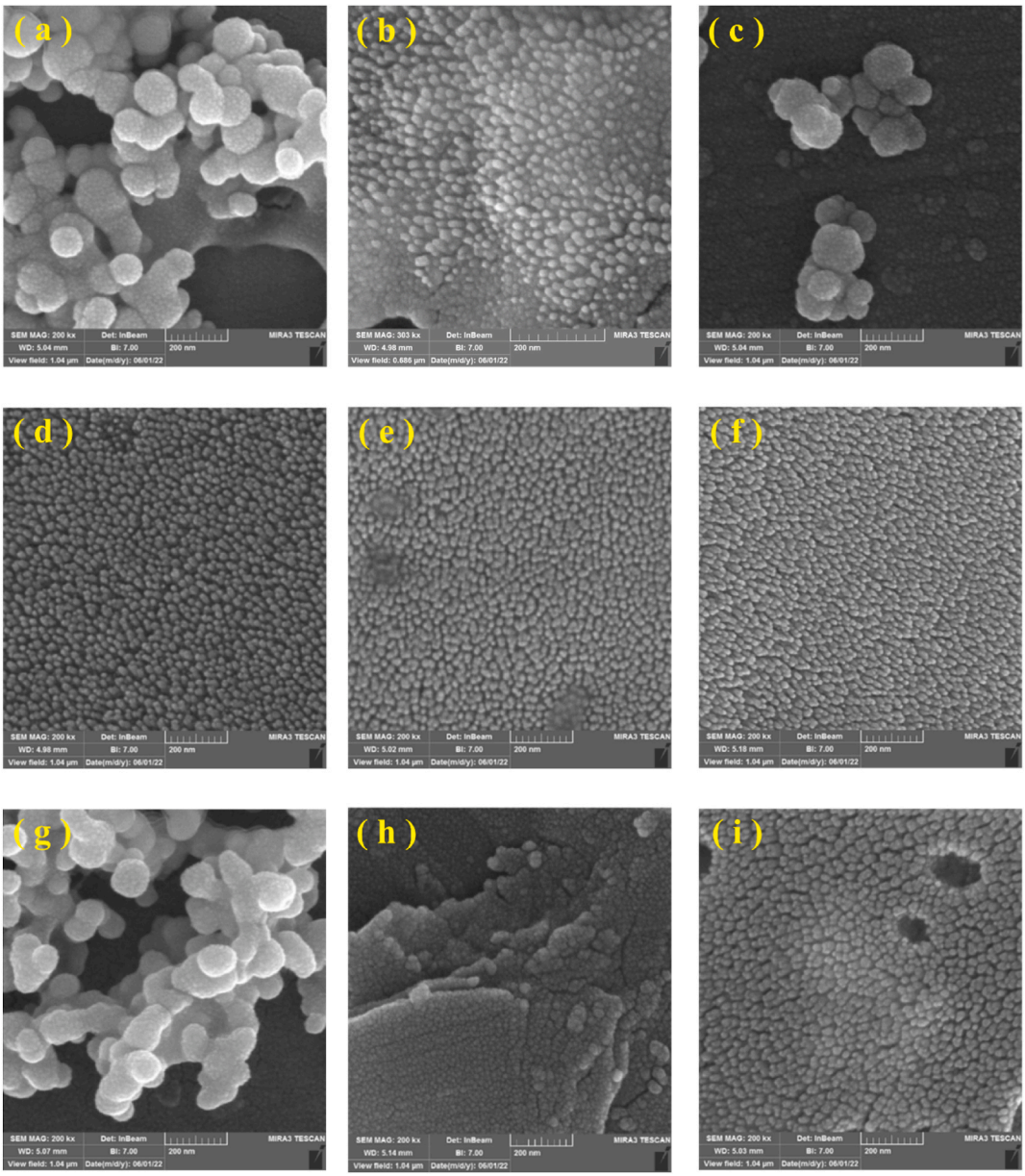

Fig. 4. FE-SEM images with codings a) P0.01H0.1, b) P0.03H0.1, c) P0.01H0.5, d) P0.03H0.5,e) P0.015H0.3, f) P0.025H0.3, g) P0.02H0.2, h) P0.02H0.4 and i) P0.02H0.3.

Table 6
Mean and standard deviation of the synthesized nanoparticles.

Samples	Mean particle size (nm)	Standard deviation (nm)
P0.01H0.1	76.11	40.8
P0.03H0.1	21.02	14.05
P0.01H0.5	66.94	37.45
P0.03H0.5	19.88	3.76
P0.015H0.3	20.38	4.19
P0.025H0.3	18.47	3.61
P0.02H0.2	41.8	24.22
P0.02H0.4	57.3	30.33
P0.02H0.3	22.12	17.54

nanoparticles could not be increased [[42–44]]. For example, the mean size of nanoparticles in P0.01H0.5 and P0.03H0.5 samples decreased from 66.94 to 19.88 nm, respectively.

Also, if the molar ratio of the stabilizer to the reductant is low, the stabilizer cannot be placed around the nanoparticles, preventing their aggregation. In addition to increasing the size of nanoparticles with a low molar ratio of stabilizer to reductant, due to the random collision of primary synthesized nanoparticles with each other and the impossibility of controlling their collision, non-uniformity in the morphology and final size of nanoparticles also occurred; as a result of the non-uniformity of the size of nanoparticles, the width of the size distribution of nanoparticles increased, causing an increase in the standard deviation [45]. In the synthesized samples, the mean size of nanoparticles was decreased from 20.38 to 18.47 by increasing the polymer stabilizer mole from 0.015 to 0.025 (considering the constant mole of the reductant at 0.3). The results obtained in the present research are, therefore, consistent with those of other studies [46]. On the other hand, in the P0.03H0.5 sample, as compared to the P0.025H0.3 one, and P0.02H0.2, as compared to the P0.02H0.4 one, the mean particle size was 19.88, 18.47, 41/3, 57/3, respectively; this showed that, due to the low molar ratio of PVP to hydrazine, the stabilizer chains could not be well placed around the nanoparticles; this was well consistent with the results obtained by other researchers [[13,47]]. As can be seen from Fig. 4(a–i), the morphology of nanoparticles was spherical or quasi-spherical. As shown in Fig. 4 (a, c, g and h), corresponding to the samples P0.01H0.1, P0.01H0.5, P0.02H0.2 and P0.02H0.4, respectively, nanoparticles had been agglomerated. According to the explanations above, due to the low molar ratio of the stabilizer to the reductant and hence, the low overlap amount of PVP for nanoparticles, there was the aggregation of nanoparticles. In general, according to the data, the sample coded P0.025H0.3 (sample 6) had the lowest mean particle size value (18.47 nm) and standard deviation (3.61). The results of the FE-SEM images also agreed with those of crystallite size in the XRD analysis; therefore, the sample 6 (P0.025H0.3) could be selected as the optimal one. The rest of the analysis and preparation of the ink containing silver nanoparticles was done with this sample; this was since, in the preparation of conductive inks, the smallest mean particle size, the narrow width of the size distribution of nanoparticles and the uniformity of distribution as the main characteristics of nanoparticles were applied. The size of nanoparticles has a direct effect on the stability, electrical conductivity and sintering temperature of the conductive ink [11]. Smaller particles are can be stabilized more easily in solution than larger particles. Due to the higher weight of large particles, it is more plausible to deposit them in the solution. Also, by reducing the size of the particles towards the nano size, the weight ratio of the filler (nanoparticles) is reduced, which leads to the easier stabilization of the nanoparticles in the conductive ink [48].

In addition, due to the high surface-to-volume ratio of nanoparticles, the connection of nanoparticles to each other is decreased and the sintering temperature is reduced, leading to a decrease in electrical resistance of the printed conductive ink [49].

3.1.3. Morphological analysis: TEM images

To complete the studies in the field of morphology and to check the size of the nanoparticles of the optimal sample (P0.025H0.3), the TEM image of the synthesized silver nanoparticles was also studied and analyzed. The TEM image of the P0.025H0.3 sample is shown in Fig. 5. According to the image, by checking the size of nanoparticles with the Digimizer software, the mean size of synthesized particles was found to be less than 20 nm and with a spherical morphology consistent with the results obtained from FE-SEM and XRD images. In the P0.025H0.3 sample, the optimum ratio of the mole of the reductant and polymer stabilizer (reductant mol/stabilizer mol = 12) reduced the size of nanoparticles, uniformity in the size distribution of nanoparticles and their distribution range.

3.1.4. Hydrodynamic particle size: DLS analysis

To determine the size of hydrodynamic particles and the scattering distribution of nanoparticles, DLS analysis was used. The results of this test for the P0.025H0.3 sample are shown in Fig. 6. The mean hydrodynamic size of nanoparticles was 34 nm and their scattering index was 0.32. The polydispersity index (PDI) of 0.32 indicated the mean scattering distribution of nanoparticles.

The size of nanoparticles obtained from DLS analysis was different from that of FE-SEM and TEM analysis; this is because DLS analysis shows the hydrodynamic diameter of nanoparticles, which includes nanoparticles along with the PVP polymer chains; according to Fig. 7, FE-SEM and TEM analyses show the real size of nanoparticles. Similar results were also observed by Balu et al. in the synthesis of silver nanoparticles. The size of nanoparticles obtained from DLS and TEM analyses was 80.66 and 39.6, respectively. The

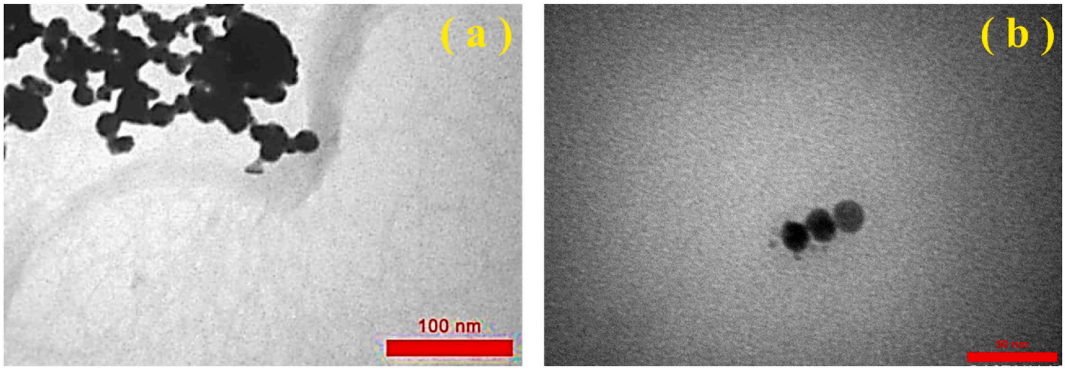

Fig. 5. TEM image of the sample having the code P0.025H0.3 with scale bars a) 100 nm and b) 50 nm.

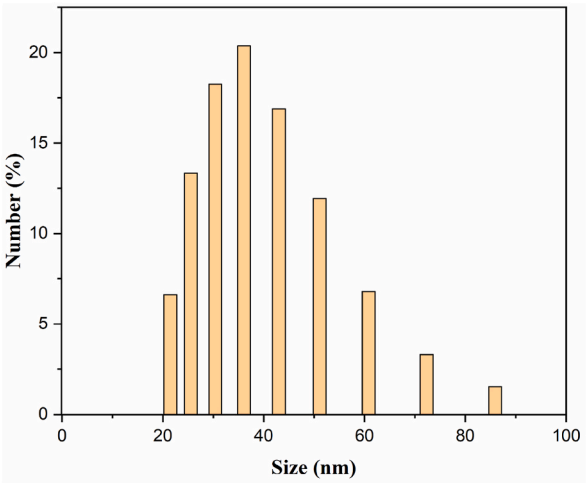

Fig. 6. Statistical diagram of the size of silver nanoparticles obtained from the DLS analysis for the sample coded P0.025H0.3.

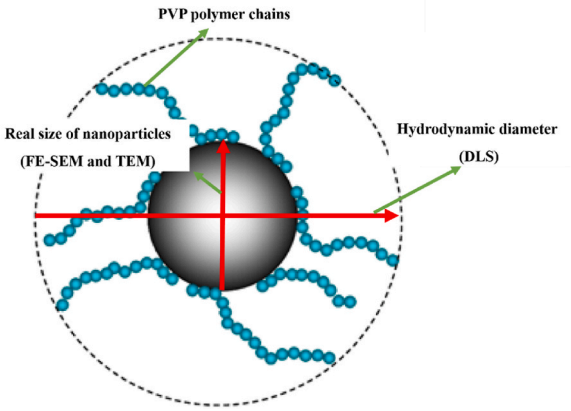

Fig. 7. The difference in measuring the size of nanoparticles by DLS (hydrodynamic diameter) analysis and FE-SEM and TEM analyses (true diameter).

reason for these changes lies in determining the hydrodynamic size and the actual size of nanoparticles by DLS and TEM, respectively [50].

3.2. Preparation of the conductive ink

3.2.1. UV–Vis analysis of the conductive silver ink

One of the common and practical methods in the structural evaluation of silver nanoparticles is the UV–Vis test, which has been used to prove the presence of silver nanoparticles in conductive ink. In general, metal nanoparticles have free electrons that show the surface plasmon resonance (SPR) due to the vibration of metal nanoparticle electrons with light waves. Silver nanoparticles have some SPR at the wavelength range of 420–400 nm. The wavelength of this characteristic peak depends on the size of the nanoparticles and the type of solution (the solution in which the nanoparticles are distributed) [51].

The UV–Vis spectrum of the conductive ink containing silver nanoparticles is shown in Fig. 8. As can be seen, the peak of the absorption spectrum of silver appeared at the wavelength of 403 nm, which confirmed the presence of silver nanoparticles in the conductive ink. In a similar study, Dang et al. observed the absorption peak of silver nanoparticles in conductive ink at the 407 nm wavelength [52].

3.2.2. STA of the conductive silver ink

The thermal behavior of conductive ink was analyzed using STA analysis. Thus, TGA and DSC were used to determine the weight percent of silver nanoparticles in the conductive ink and the reactions occurring in the conductive ink, respectively. The TGA and DSC diagram is presented in Fig. 9. According to the TGA curve; it was observed that weight loss began at 50 °C and ended at 194 °C. This weight loss indicated the evaporation of ethylene glycol and ethanol, which was associated with 61 %wt mass loss. Therefore, the

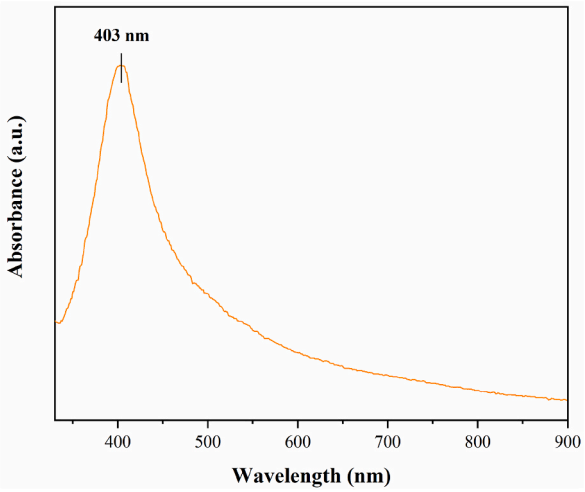

Fig. 8. UV–Vis spectrum of the conductive silver ink.

remaining mass was 39%, indicating the remaining silver nanoparticles, which showed the weight percent of the filler of the silver nanoparticles in the conductive ink. In addition, the concentration of silver nanoparticles in conductive ink was determined by AAS measurement. The concentration obtained by AAS analysis for the conductive silver ink was equal to 400,000 ppm. The results related to the remaining weight percent resulting from TGA well agreed with the calculated amount of silver nanoparticles in ink (40%).

The DSC curve also showed an endothermic peak of 137 °C that was related to the evaporation of the solvents. An exothermic peak also occurred at 194 °C, which was associated with the end of the reaction. According to other researchers, the neck growth and sintering of nanoparticles that cause the surface penetration of unstable atoms into each other are accompanied by an exothermic peak [[53,54]].

3.2.3. Printed silver conductive ink characterization and analysis

After preparing the ink, a pattern and layer were applied to the PET and ABS substrates, and sintering was done at 110 °C (Fig. 10). Silver conductive ink was applied to the PET substrate by silk screen and on the ABS substrate through the spray method.

As can be seen, the ink printed on PET and ABS had the electrical resistance of 4.6 and 2.2 Ω. The multimeter probe distance and the measured area could affect the surface electrical resistance of the printed ink. Yamada et al. and Li et al. also obtained the electrical resistance of the printed silver ink on the PET substrate and paper after sintering at 80 °C and °C 140, which was equal to 4.2 Ω [[55, 56]].

The adhesion strength of conductive ink printed on PET and ABS substrates was evaluated by the detached strip test and classified into 0B–5B classes. Based on the areas separated by six parallel cuts, the adhesion of printed ink on PET and ABS substrates was classified into 2B and 4B classes, respectively. The higher adhesion of ABS was due to its higher surface roughness, as compared to PET, which would leadto a stronger mechanical bond between the substrate and the conductive ink by penetrating the conductive ink in the pores of the ABS substrate [[35,53]].

FE-SEM images of the sintered silver conductive ink layer on the ABS and PET substrates are shown in Fig. 11. As can be seen, the bonding of nanoparticles in the conductive ink sintered on the ABS substrate (Fig. 11a) was found to be higher than that on the PET substrate (Fig. 11b), and more nanoparticles were connected due to sintering. The better sintering of nanoparticles on the ABS substrate than on the PET one couldbe related to the stronger mechanical bond of the conductive ink with the ABS substrate. For this reason, the better connection of nanoparticles to each other and higher uniformity in the conductive coating on the ABS substrate could lead to its higher electrical conductivity, as compared to the PET substrate.

The printed layer microstructure showed the integration process between nanoparticles after sintering due to the evaporation of organic compounds. Empty spaces were also due to the evaporation of solvents and volatile organic matter. The adjacent silver nanoparticles were melted, forming larger particles through the neck growth mechanism. The neck growth of adjacent nanoparticles in sintering is mainly by grain boundary and surface distributions. Due to the high specific surface area and the effect of the small size of the nanoparticles, the surface and grain boundary activation of nanoparticles can besignificantly higher than that of the bulk materials useful for surface emission and grain boundary distribution. For this reason, the sintering of the metal nanoparticles is possible at temperatures below the bulk melting temperature due to the high surface-to-volume ratio, thus reducing the melting temperature. After the complete evaporation of the solvent and the remains of organic matter that prevented direct contact with nanoparticles, it resulted in penetration and neck growth between nanoparticles. These coarse grains could provide more electron transmission paths, thus playing an important role in reducing electrical resistance. Other researchers have also confirmed the mechanisms occurring during the sintering of nanoparticles [57].

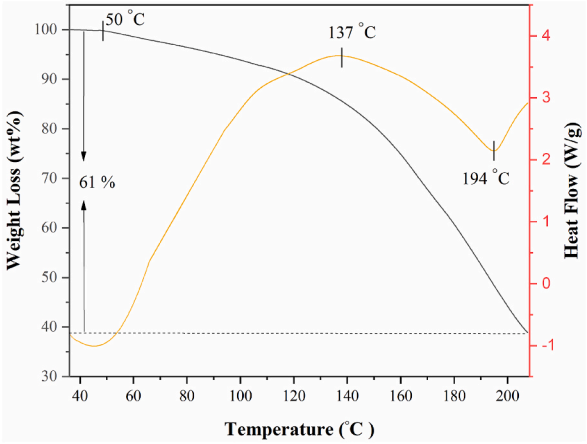

Fig. 9. TGA and DSC diagrams of silver conductive ink.

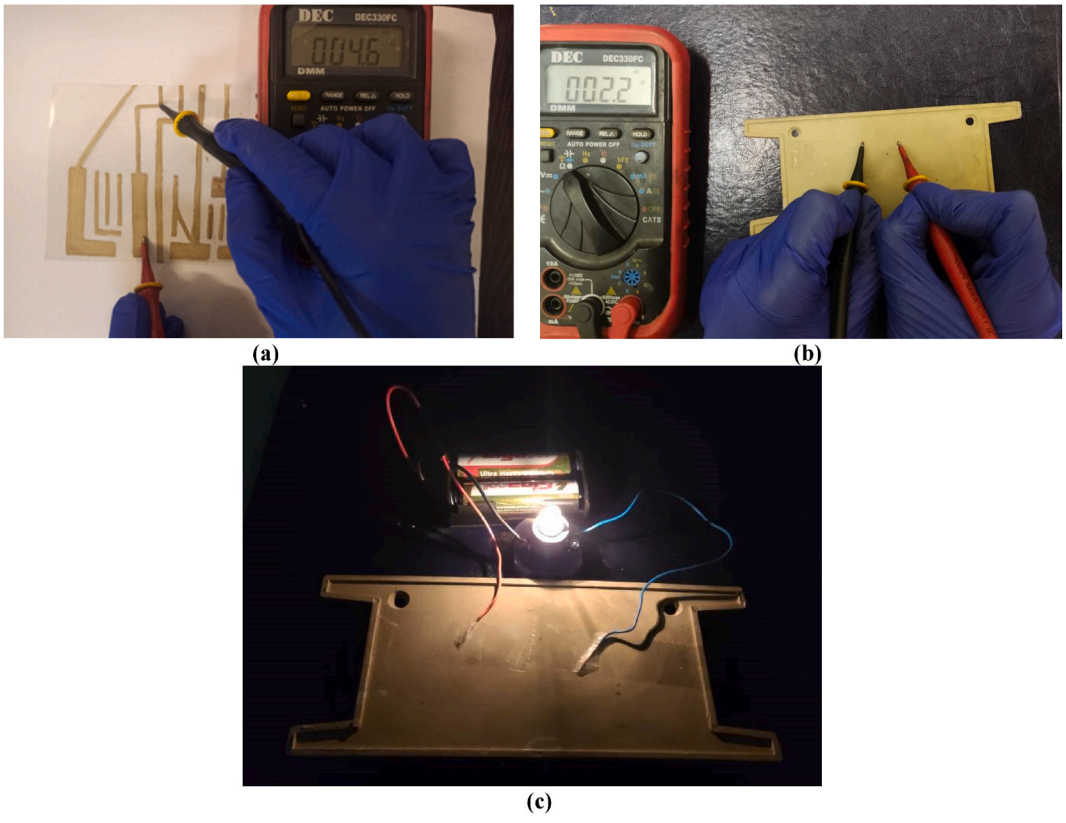

Fig. 10. Sintered silver conductive ink at 110 °C for a) the pattern printed on the PET substrate, b) sprayed conductive ink on the ABS substrate and c) lighting to indicate electrical conductivity on the ABS substrate.

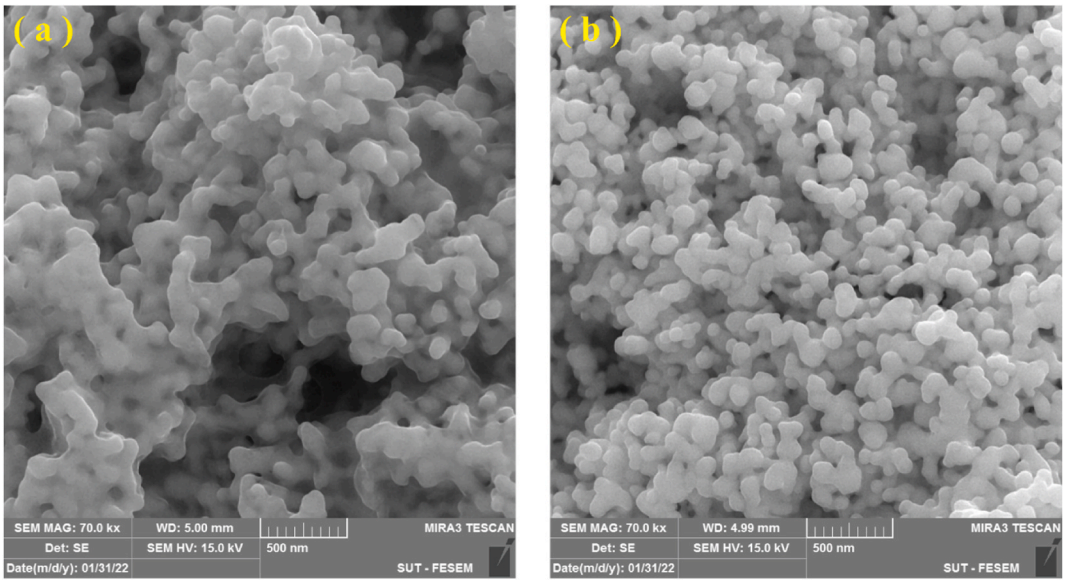

Fig. 11. FE-SEM image of the coating surface of the conductive ink sintered at 110 °C on a) ABS and b) PET substrates.

4. Conclusion

The synthesis of silver nanoparticles was performed by the chemical reduction method. Accordingly, and nine random samples specified by the Expert Design were software synthesized and studied. Then, by using the optimized sample, the silver nanoparticles were distributed in ethanol and ethylene solvents and the conductive ink containing silver nanoparticles was prepared. The most important results from this study can be summarized as follows:

- In the XRD pattern of silver nanoparticles synthesized in any of the samples, the oxide peak was not identified and the size of the crystallites from the samples was 18.7–37.4 nm. The least amount of crystallite size was for the sample P0.025H0.3, with the ratio of reductant mol/stabilizer mol being 12.
- Accoriding to the FE-SEM images, the optimized sample, coded P0.025H0.3, due to the appropriateness of the mole ratio of hydrazine reductant to PVP stabilizer, resulted in the reduction of the mean and standard deviation of silver nanoparticles to 18.47, and 3.61 nm, respectively.
- TEM image showed the spherical or quasi-spherical morphology of silver nanoparticles with a size of 20 nm, which was in a good agreement with the results obtained by the XRD pattern and FE-SEM.
- The hydrodynamic diameter of the silver nanoparticles (PVP chains + Ag nanoparticles), using DLS, was calculated to be 34 nm and its polydispersity index (PDI) was equal to 0.32.
- The UV–Vis diagram of silver conductive ink in the wavelength area showed a 403 nm peak of silver absorption, thus indicating the presence of silver nanoparticles in the conductive ink.
- TGA of the conductive ink indicated a weight loss of 61% and the presence of 39% of the weight of silver nanoparticles in the conductive ink, which was compatible with the calculated theory weight percent. DSC also showed an endothermic peak at 137 °C (caused by the evaporation of solvents) and an exothermic peak at 194 °C (due to the end of the reaction and the surface penetration of the atoms).
- The surface electrical resistance of conductive ink applied on PET and ABS substrates and sintered at 110 °C was measured as 6.4 and 2.2 using a multimeter, respectively.
- FE-SEM image obtained from the surface of the conductive ink coating applied to the ABS layer and sintered at 110 °C indicated the dense structure, the good connection of the nanoparticles to each other, and the proper growth of the nanoparticles after sintering.

Author contribution statement

Ehsan Naderi-Samani: Conceived and designed the experiments; Performed the experiments; Analyzed and interpreted the data; Contributed reagents, materials, analysis tools or data; Wrote the paper.

Reza Shoja Razavi; Khanali Nekouee; Hamed Naderi-Samani: Conceived and designed the experiments; Contributed reagents, materials, analysis tools or data.

Data availability statement

The authors are unable or have chosen not to specify which data has been used.

Declaration of competing interest

The authors declare that they have no known competing financial interests or personal relationships that could have appeared to influence the work reported in this paper.

References

[1] J. Wiklund, A. Karakoç, T. Palko, H. Yiğitler, K. Ruttik, R. Jäntti, J. Paltakari, A review on printed electronics: fabrication methods, inks, substrates, applications and environmental impacts, Journal of Manufacturing and Materials Processing 5 (2021) 89.
[2] V. Scenev, J. Szalapak, L. Werft, O. Hoelck, M. Jakubowska, M. von Krshiwoblozki, C. Kallmayer, M. Schneider-Ramelow, Low-temperature processible highly conducting pastes for printed electronics applications, Adv. Eng. Mater. 24 (2022), 2101752.
[3] Y. Bonnassieux, C.J. Brabec, Y. Cao, T.B. Carmichael, M.L. Chabinyc, K.-T. Cheng, G. Cho, A. Chung, C.L. Cobb, A. Distler, The 2021 flexible and printed electronics roadmap, Flexible and printed electronics 6 (2021), 023001.
[4] X. Gong, K. Huang, Y.-H. Wu, X.-S. Zhang, Recent progress on screen-printed flexible sensors for human health monitoring, Sensor Actuator Phys. (2022), 113821.
[5] V. Beedasy, P.J. Smith, Printed electronics as prepared by inkjet printing, Materials 13 (2020) 704.
[6] C.P. Buga, J.C. Viana, The Role of Printed Electronics and Related Technologies in the Development of Smart Connected Products, Flexible and Printed Electronics, 2022.
[7] T.M. Prenzel, F. Gehring, Z.J. Davis, N. Slack, I. Katsavou, L.H. Jakobsen, C. Fito, N. Hvid, J. Serrano, Accelerating Sustainable Development and Production of Nanomaterials and Printed Electronics, E3S Web of Conferences, EDP Sciences, 2022, 11007.
[8] G.B. Hong, Y.H. Luo, K.J. Chuang, H.Y. Cheng, K.C. Chang, C.M. Ma, Facile synthesis of silver nanoparticles and preparation of conductive ink, Nanomaterials 12 (2022) 171.
[9] Z. Ma, X. Jiang, Y. Jin, M. Wu, L. Wang, Preparation of nano-silver nanoparticles for conductive ink and the correlations with its conductivity, Appl. Nanosci. 12 (2022) 1657–1665.
[10] J. Zhang, M. Ahmadi, G. Fargas, N. Perinka, J. Reguera, S. Lanceros-Méndez, L. Llanes, E. Jiménez-Piqué, Silver nanoparticles for conductive inks: from synthesis and ink formulation to their use in printing technologies, Metals 12 (2022) 234.
[11] E. Dimitriou, N. Michailidis, Printable conductive inks used for the fabrication of electronics: an overview, Nanotechnology 32 (2021), 502009.
[12] L. Ramajo, R. Parra, M. Reboredo, M. Castro, Preparation of amine coated silver nanoparticles using triethylenetetramine, Journal of chemical sciences 121 (2009) 83–87.
[13] T.M.D. Dang, T.T.T. Le, E. Fribourg-Blanc, M.C. Dang, Influence of surfactant on the preparation of silver nanoparticles by polyol method, Adv. Nat. Sci. Nanosci. Nanotechnol. 3 (2012), 035004.
[14] N. Samadi, S. Hosseini, A. Fazeli, M. Fazeli, Synthesis and antimicrobial effects of silver nanoparticles produced by chemical reduction method, Daru 18 (2010) 168.
[15] M. Alqadi, O. Abo Noqtah, F. Alzoubi, J. Alzouby, K. Aljarrah, pH effect on the aggregation of silver nanoparticles synthesized by chemical reduction, Materials Science-Poland 32 (2014) 107–111.
[16] A. Amany, S.F.G. El-Rab, F. Gad, Effect of reducing and protecting agents on size of silver nanoparticles and their anti-bacterial activity, Der Pharma Chem. 4 (2012) 53–65.
[17] M. Sadjadi, B. Sadeghi, M. Meskinfam, K. Zare, J. Azizian, Synthesis and characterization of Ag/PVA nanorods by chemical reduction method, Phys. E Low-dimens. Syst. Nanostruct. 40 (2008) 3183–3186.
[18] A. Sobczak-Kupiec, D. Malina, Z. Wzorek, M. Zimowska, Influence of silver nitrate concentration on the properties of silver nanoparticles, Micro & Nano Lett. 6 (2011) 656–660.
[19] P. Van Dong, C.H. Ha, L.T. Binh, J. Kasbohm, Chemical synthesis and antibacterial activity of novel-shaped silver nanoparticles, Int. Nano Lett. 2 (2012) 1–9.
[20] A.J. Kora, L. Rastogi, Enhancement of antibacterial activity of capped silver nanoparticles in combination with antibiotics, on model gram-negative and gram-positive bacteria, Bioinorg. Chem. Appl. 2013 (2013) 1–7.
[21] M. Bin Ahmad, J.J. Lim, K. Shameli, N.A. Ibrahim, M.Y. Tay, Synthesis of silver nanoparticles in chitosan, gelatin and chitosan/gelatin bionanocomposites by a chemical reducing agent and their characterization, Molecules 16 (2011) 7237–7248.
[22] Z. Jia, H. Sun, Q. Gu, Preparation of Ag nanoparticles with triethanolamine as reducing agent and their antibacterial property, Colloids Surf. A Physicochem. Eng. Asp. 419 (2013) 174–179.
[23] K.-S. Chou, Y.-S. Lai, Effect of polyvinyl pyrrolidone molecular weights on the formation of nanosized silver colloids, Mater. Chem. Phys. 83 (2004) 82–88.
[24] J. Xiong, X.-d. Wu, Q.-j. Xue, One-step route for the synthesis of monodisperse aliphatic amine-stabilized silver nanoparticles, Colloids Surf. A Physicochem. Eng. Asp. 423 (2013) 89–97.
[25] R.S. Patil, M.R. Kokate, C.L. Jambhale, S.M. Pawar, S.H. Han, S.S. Kolekar, One-pot synthesis of PVA-capped silver nanoparticles their characterization and biomedical application, Adv. Nat. Sci. Nanosci. Nanotechnol. 3 (2012), 015013.
[26] P. Aminayi, B. Young, T. Young, L. Sprowl, M. Joyce, Inkjet printing and surface treatment of an optimized polyurethane-based ink formulation as a suitable insulator over silver for contact with aqueous-based fluids in low-voltage applications, J. Coating Technol. Res. 14 (2017) 641–649.
[27] M. Hösel, F.C. Krebs, Large-scale roll-to-roll photonic sintering of flexo printed silver nanoparticle electrodes, J. Mater. Chem. 22 (2012) 15683–15688.
[28] T. Schönfelder, F. Kemper, L. Pohle, M. Reif, M. Tienken, E. Beckert, A. Tünnermann, Inkjet Printing of Dielectric Layers with High Relative Permittivity for Digital Microfluidics, Microfluidics, BioMEMS, and Medical Microsystems XIX, SPIE, 2021, pp. 18–22.
[29] Emi Shielding, PRO-SHIELD 7108 Electrically Conductive Silver Acrylic Paint, https://ph.parker.com/us/en/series/emi-shielding-paints..
[30] S. Kasim, S. Dali, M. Rahmah, Synthesis of silver nanoparticles using bioreductors from clove leaf extract (Syzygium aromaticum) and test of its antibacterial activity, J. Phys.: Conference Series, IOP Publishing (2021), 012051.
[31] J.M. Berg, Principles of Bioinorganic Chemistry, University Science Books, 1994.
[32] D. Cheng, S. Xia, J. Tong, The mechanism of directional oxidation of hydrazine by silver coordination compounds, Transit. Met. Chem. 21 (1996) 503–506.
[33] W.T. Hall, Oxidation-reduction reactions, J. Chem. Educ. 6 (1929) 479.
[34] A.E. Martell, R.D. Hancock, Metal Complexes in Aqueous Solutions, Springer Science & Business Media, 2013.
[35] H. Naderi-Samani, R.S. Razavi, M.R. Loghman-Estarki, M. Ramazani, The effects of organoclay on the morphology and mechanical properties of PAI/clay nanocomposites coatings prepared by the ultrasonication assisted process, Ultrason. Sonochem. 38 (2017) 306–316.
[36] P.F. de Oliveira, A.A. Michalchuk, J. Marquardt, T. Feiler, C. Prinz, R.M. Torresi, P.H. Camargo, F. Emmerling, Investigating the role of reducing agents on mechanosynthesis of Au nanoparticles, CrystEngComm 22 (2020) 6261–6267.
[37] N.A.N. Mohamad, N.A. Arham, J. Jai, A. Hadi, Plant extract as reducing agent in synthesis of metallic nanoparticles: a review, Adv. Mater. Res. 832 (2014) 350–355.

[38] Z. Yi, X. Li, X. Xu, B. Luo, J. Luo, W. Wu, Y. Yi, Y. Tang, Green, effective chemical route for the synthesis of silver nanoplates in tannic acid aqueous solution, Colloids Surf. A Physicochem. Eng. Asp. 392 (2011) 131–136.
[39] G. Cao, Nanostructures & Nanomaterials: Synthesis, Properties & Applications, Imperial college press, 2004.
[40] B.K. Park, S. Jeong, D. Kim, J. Moon, S. Lim, J.S. Kim, Synthesis and size control of monodisperse copper nanoparticles by polyol method, J. Colloid Interface Sci. 311 (2007) 417–424.
[41] H. Zhang, C. Zhang, Transport of silver nanoparticles capped with different stabilizers in water saturated porous media, J. Mater. Environ. Sci. 5 (2014) 231–236.
[42] K.-Y. Kim, M.-S. Gong, C.-K. Park, Preparation of highly stabilized silver nanopowders by the thermal reduction and their properties, Bull. Kor. Chem. Soc. 33 (2012) 3987–3992.
[43] D. Malina, A. Sobczak-Kupiec, Z. Wzorek, Z. Kowalski, Silver nanoparticles synthesis with different concentrations of polyvinylpyrrolidone, Dig. J. Nanomater. Biostruct. 7 (2012).
[44] K. Shameli, M.B. Ahmad, S.D. Jazayeri, S. Sedaghat, P. Shabanzadeh, H. Jahangirian, M. Mahdavi, Y. Abdollahi, Synthesis and characterization of polyethylene glycol mediated silver nanoparticles by the green method, Int. J. Mol. Sci. 13 (2012) 6639–6650.
[45] M. Li, Y.-T. Li, D.-W. Li, Y.-T. Long, Recent developments and applications of screen-printed electrodes in environmental assays—a review, Anal. Chim. Acta 734 (2012) 31–44.
[46] H.-t. Zhu, C.-y. Zhang, Y.-s. Yin, Rapid synthesis of copper nanoparticles by sodium hypophosphite reduction in ethylene glycol under microwave irradiation, J. Cryst. Growth 270 (2004) 722–728.
[47] D. Chen, X. Qiao, X. Qiu, J. Chen, Synthesis and electrical properties of uniform silver nanoparticles for electronic applications, J. Mater. Sci. 44 (2009) 1076–1081.
[48] H. Naderi-Samani, R.S. Razavi, M. Loghman-Estarki, M. Ramazani, M. Barekat, A. Mishra, H. Fattahi, The effects of Cloisite 20A content on the adhesion strength and corrosion behavior of poly (amide-imide)/cloisite 20A nanocomposite coatings, Compos. B Eng. 175 (2019), 107154.
[49] Z. Cui, Printed Electronics: Materials, Technologies and Applications, John Wiley & Sons, 2016.
[50] S. Balu, S. Andra, S. Kannan, M. Muthalagu, Facile synthesis of silver nanoparticles with medicinal grass and its biological assessment, Mater. Lett. 259 (2020), 126900.
[51] C.V. Restrepo, C.C. Villa, Synthesis of silver nanoparticles, influence of capping agents, and dependence on size and shape: a review, Environ. Nanotechnol. Monit. Manag. 15 (2021), 100428.
[52] M.C. Dang, T.M.D. Dang, E. Fribourg-Blanc, Silver nanoparticles ink synthesis for conductive patterns fabrication using inkjet printing technology, Adv. Nat. Sci. Nanosci. Nanotechnol. 6 (2014), 015003.
[53] H. Naderi-Samani, R.S. Razavi, R. Mozaffarinia, The effects of complex agent and sintering temperature on conductive copper complex paste, Heliyon (2022), e12624.
[54] K. Woo, D. Kim, J.S. Kim, S. Lim, J. Moon, Ink-Jet printing of Cu− Ag-based highly conductive tracks on a transparent substrate, Langmuir 25 (2009) 429–433.
[55] W. Li, X. Xu, W. Li, Y. Zhao, M. Chen, Green synthesis of micron-sized silver flakes and their application in conductive ink, J. Mater. Sci. 53 (2018) 6424–6432.
[56] T. Yamada, K. Fukuhara, K. Matsuoka, H. Minemawari, J.y. Tsutsumi, N. Fukuda, K. Aoshima, S. Arai, Y. Makita, H. Kubo, Nanoparticle chemisorption printing technique for conductive silver patterning with submicron resolution, Nat. Commun. 7 (2016), 11402.
[57] Z. Liu, H. Ji, S. Wang, W. Zhao, Y. Huang, H. Feng, J. Wei, M. Li, Enhanced electrical and mechanical properties of a printed bimodal silver nanoparticle ink for flexible electronics, physica status solidi (a) 215 (2018), 1800007.